Electrical Capacitance Tomography Measurements on the Pneumatic Conveying of Solids

S. Madhusudana Rao,[†] Kewu Zhu,[†] Chi-Hwa Wang,*[,†] and Sankaran Sundaresan[‡]

Department of Chemical and Environmental Engineering, National University of Singapore, 4 Engineering Drive 4, Singapore 117576, and Department of Chemical Engineering, Princeton University, Princeton, New Jersey 08544

We have evaluated the usefulness of electrical capacitance tomography (ECT) as a tool for monitoring pneumatic conveying in horizontal ducts. Power spectra of solids concentration fluctuations obtained from single-plane ECT data were used to identify the various flow regimes, and these were confirmed through visual observation. From single-plane ECT data, the instantaneous and time-averaged distributions of particle concentration over the cross section of the conveying pipe have been determined in various flow regimes. Propagation velocities of patterns were evaluated from cross correlation of twin-plane ECT data. The solids mass flow rate, determined independently by load cell measurements, was found to be roughly proportional to the product of the pattern velocity, the particle density, and the average solids holdup in the pipe, and the proportionality factor depended on the material being transported through the pipe. In our experiments involving flows past a 90° smooth bend, ECT was able to detect significant temporal and spatial nonuniformity in particle concentration in the postbend region.

Introduction

There is a practical need for on-line monitoring, metering, and control of pneumatic conveying operations, and electrical capacitance tomography (ECT) is emerging as a potential noninvasive tool for this purpose. ECT[1−5] is a noninvasive technique to image dielectric components in pipes or vessels. The tomography results may be used for process visualization, control, malfunction detection, and troubleshooting. The capacitance across a given pair of electrodes depends on the geometric configuration of the electrodes and the global average dielectric property of the material occupying the entire sensing volume, and it can be used to probe the composition of multicomponent mixtures.[1−5] By placing multiple electrode sensors around the circumference of a pipe and measuring the capacitances between the various pairs of electrodes, one can generate the information needed to estimate the variation of the mixture composition over the cross section of the pipe. The resolution of the image depends on the design of the sensor (length of the electrode and spacing between them) and the thickness of test pipe and its material. ECT is simply such a measurement system and the associated software for inverting the capacitance data to obtain the desired image. By repeating such measurements at a sequence of times, one can determine the temporal variation of the spatial distribution of composition. McKee et al.[4] have described the application of the ECT technique to monitor the behavior of industrial-scale pneumatic conveyors. Through cross correlation of time-dependent data obtained at two sets of electrodes located at two different axial locations in a pipe (commonly referred to as twin-plane sensors), one can learn about the speed at which disturbances propagate through the pipe.

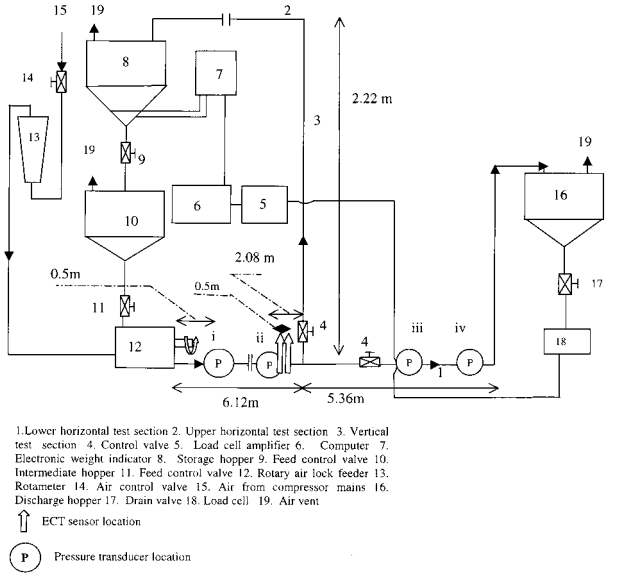

Figure 1. Schematic layout of the experimental facility.

Table 1. Physical Properties of Particles (All Geldart D Type)

material	diameter (mm)	density (kg/m^3)
titanium dioxide filled LLDPE	3.01	1683
brown mustard (Brassica Juncea)	1.76	879
polypropylene	2.80	1123

Arko et al.[6] have demonstrated the use of the ECT system for the solids flow metering in one of the flow regimes, namely, slug flow. From ECT measurements, they were able to determine the average volume fraction of particles in the pipe by averaging over both time and cross section. Through cross correlation of the twin-plane ECT signals, they determined the pattern velocity (defined as the propagation velocity of density nonuniformities) and obtained an estimate of the average solids volume flux as the product of the pattern velocity, the average volume fraction of particles mentioned above,

* Corresponding author. Telephone: 65-874-5079. Fax: 65-779-1936. E-mail: chewch@nus.edu.sg.
[†] National University of Singapore.
[‡] Princeton University.

10.1021/ie0100028 CCC: $20.00
Published on Web 05/18/2001

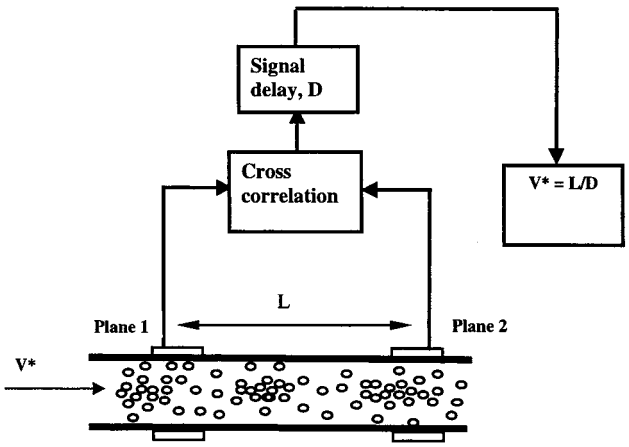

Figure 2. Twin-plane ECT system for the velocity measurement.

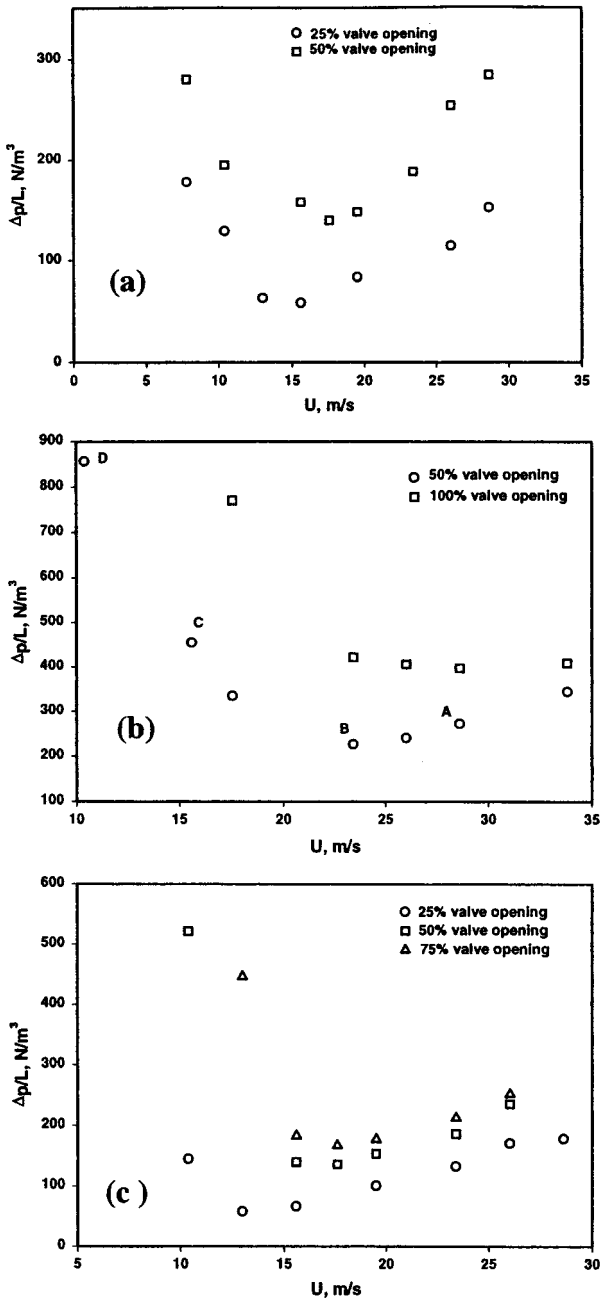

Figure 3. Pneumatic conveying characteristics in a horizontal pipe. The pressure gradient is plotted against the superficial gas velocity for different values of solids mass flux: (a) brown mustard; (b) LLDPE; (c) polypropylene. Also see Tables 2−4.

Table 2. Pressure Gradient Data for Brown Mustard Particles[a]

U (m/s)	G_s (kg/m^2·s)	$\Delta P/L$ (Pa/m)	regime
28.6	11.5	152.4	H
26.0	11.2	114.2	H
19.5	11.9	83.3	S
15.6	12.3	58.1	S/MD
13.0	12.0	63.0	MD
10.4	12.0	129.2	ED
7.8	12.6	178.3	FSL
28.6	47.9	283.6	H
26.0	48.2	253.4	H/S
23.4	48.5	187.9	S
19.5	48.3	147.8	S
17.6	48.6	139.5	MD
15.6	48.6	157.9	MD/ED
10.4	29.7	195.2	ED/FSL
7.8	19.4	279.8	FSL

[a] H = homogeneous flow; H/S = transition from homogeneous to stratified flow; S = stratified flow; S/MD = transition from stratified to moving dunes; MD = moving dunes; MD/ED = transition from moving dunes to eroding dunes; ED = eroding dunes; ED/FSL = transition from eroding dunes to flow over a settled layer; FSL = flow over a settled layer.

Table 3. Pressure Gradient Data for LLDPE Particles[a]

U (m/s)	G_s (kg/m^2·s)	$\Delta P/L$ (Pa/m)	regime
33.8	70.1	343.9	H
28.6	71.4	271.4	H
26.0	72.3	239.6	H/MD
23.4	73.6	225.1	MD
17.6	25.2	334.1	ED/FSL
15.6	17.2	454.0	FSL
10.4	21.1	855.6	SF
33.8	130.2	408.8	H
28.6	128.8	397.3	S
26.0	125.4	405.8	S
23.4	126.2	421.4	MD
17.6	26.5	769.8	ED/FSL

[a] H = homogeneous flow; S = stratified flow; H/MD = transition from homogeneous to moving dunes; MD = moving dunes; ED/FSL = transition from eroding dunes to flow over a settled layer; FSL = flow over a settled layer; SF = slug flow.

Table 4. Pressure Gradient Data for Polypropylene Particles[a]

U (m/s)	G_s (kg/m^2·s)	$\Delta P/L$ (Pa/m)	regime
28.6	15.5	177.8	H
26.0	13.4	170.8	H
23.4	13.5	132.3	H
19.5	14.7	100.5	H
15.6	14.2	66.4	H
13.0	13.2	57.5	S/MD
10.4	11.1	144.3	ED/FSL
26.0	50.6	235.5	H
23.4	50.1	186.2	H
19.5	50.2	153.7	H/MD
17.6	50.7	135.8	MD
15.6	49.7	139.8	MD
10.4	37.8	522.0	SD/SF
26.0	93.7	251.8	H
23.4	94.0	212.4	H
19.5	93.2	177.4	H/MD
17.6	92.7	167.1	MD
15.6	78.4	183.1	ED
13.0	38.7	446.3	SD

[a] H = homogeneous flow; H/MD = transition from homogeneous flow to moving dunes; S/MD = transition from stratified flow to moving dunes; MD = moving dunes; ED/FSL = transition from eroding dunes to flow over a settled layer; ED = eroding dunes; FSL = flow over a settled layer; SD = sweeping dunes; SD/SF = transition from sweeping dunes to slug flow.

and an empirical "intermittency factor". This intermittency factor is necessary because the average particle velocity need not be equal to the pattern velocity, and

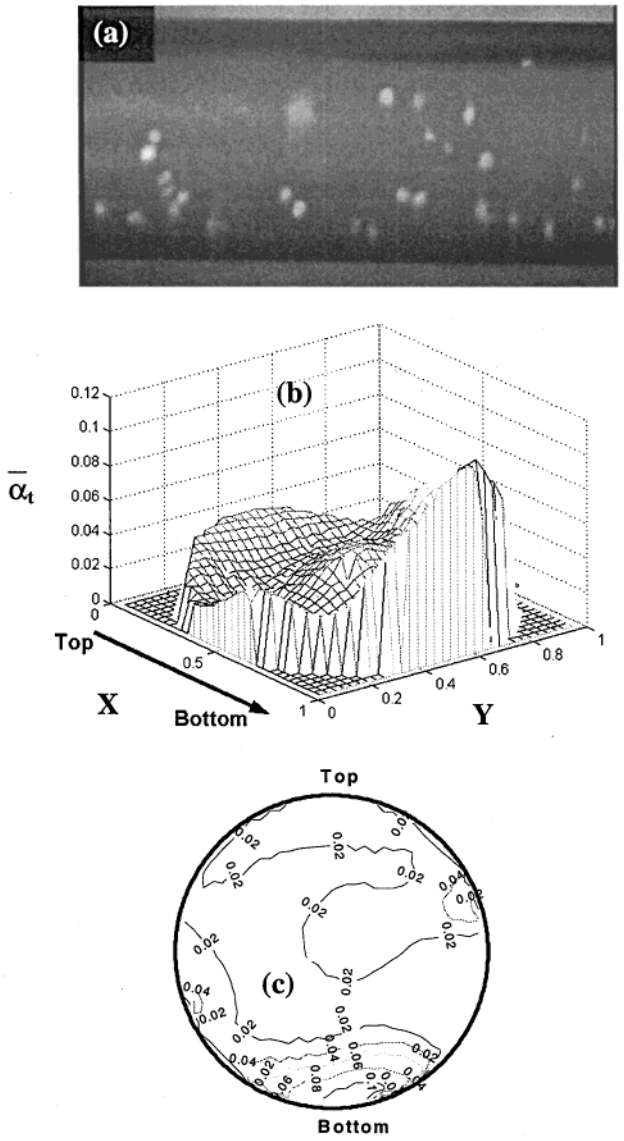

Figure 4. Homogeneous flow regime. Air superficial velocity U = 28.6 m/s. Solids feed rate G_s = 71.4 kg/m^2·s (valve opening = 50%, point A in Figure 3b). LLDPE particles: (a) typical flow pattern captured by a video camera; (b) surface plot of time-averaged particle concentration, $\bar{\alpha}_t$; (c) contour plot of $\bar{\alpha}_t$.

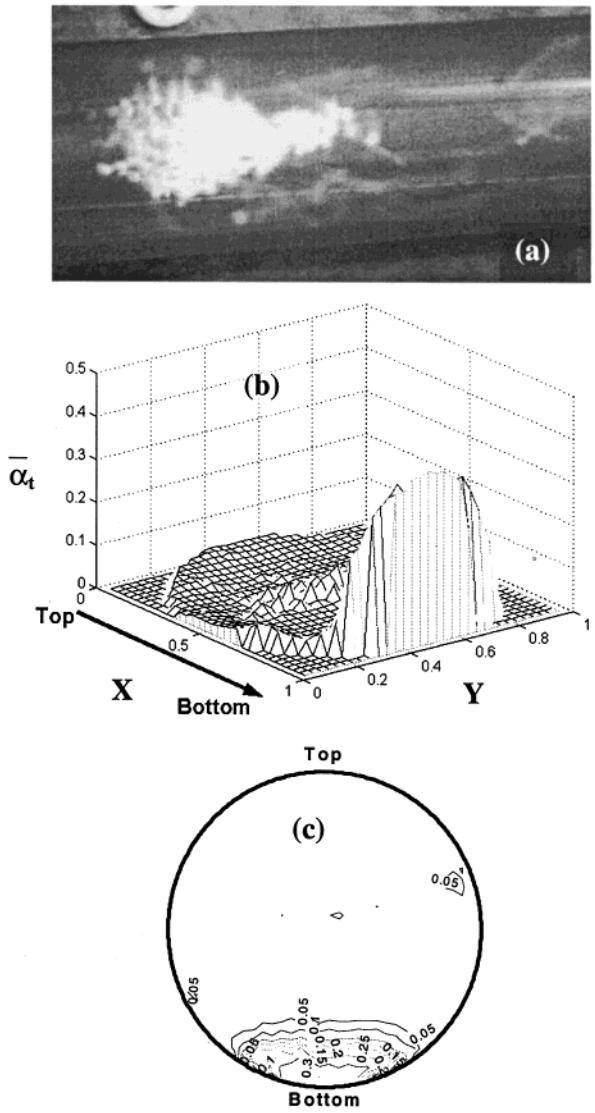

Figure 5. Moving dunes flow regime. Air superficial velocity U = 23.4 m/s. Solids feed rate G_s = 73.6 kg/m^2·s (valve opening = 50%, point B in Figure 3b). LLDPE particles: (a) typical flow pattern captured by a video camera; (b) surface plot of time-averaged particle concentration, $\bar{\alpha}_t$; (c) contour plot of $\bar{\alpha}_t$.

the slug flow is inherently intermittent. It is not known at this time if such an empirical factor will work well for flow patterns other than slug flow.

The dynamic nature of the pneumatic conveying of solids in a pipe has inspired many researchers to diagnose the flow behavior by studying the fluctuations. Tsuji and Morikawa[7] studied the pneumatic transport of plastic pellets (0.19 and 2.8 mm diameter) in a horizontal pipe (40 mm i.d.) and established a relation between flow patterns and pressure fluctuations (<10 Hz). The superficial air velocities were less than 14 m/s. They considered five different flow patterns, namely, homogeneous flow, moving dunes, blowing clusters, flow over a settled layer, and slug flow. The power spectrum of the homogeneous flow was typically characterized by high-frequency (>∼1 Hz) fluctuations, while in the moving clusters regime (also known as moving dunes), they were in the range of 0.1−1 Hz for both small and large particles. In the case of blowing clusters, the dominant frequency was ∼0.1 Hz (for small particles). The power spectrum for flow over a settled layer was similar to that of the moving clusters, while that for the slug flow of large particles had a sharp peak at low-frequency values (∼0.2 Hz).

Dhodapkar and Klinzing[8] measured pressure fluctuations (up to 200 Hz) accompanying horizontal pneumatic conveying of 55 and 450 μm glass beads. They showed that in the homogeneous flow regime, obtained at low solids flow rate and moderate gas flow rate, the addition of particles led to an attenuation of high-frequency fluctuations for the 450 μm glass beads. In contrast, the 55 μm glass beads created a distinct band around 5 Hz.

Matsumoto and Harakawa[9] have quantitatively described flow regimes for vertical pneumatic conveying using the solids concentration fluctuations determined using a photosensor. The power spectral function of the solids concentration fluctuations described very well the flow regime transition from a suspended bed to the slug flow.

In the present study, experiments have been performed over a wide range of flow regimes using three types of particles, namely, titanium dioxide filled linear low-density polyethylene (LLDPE), brown mustard

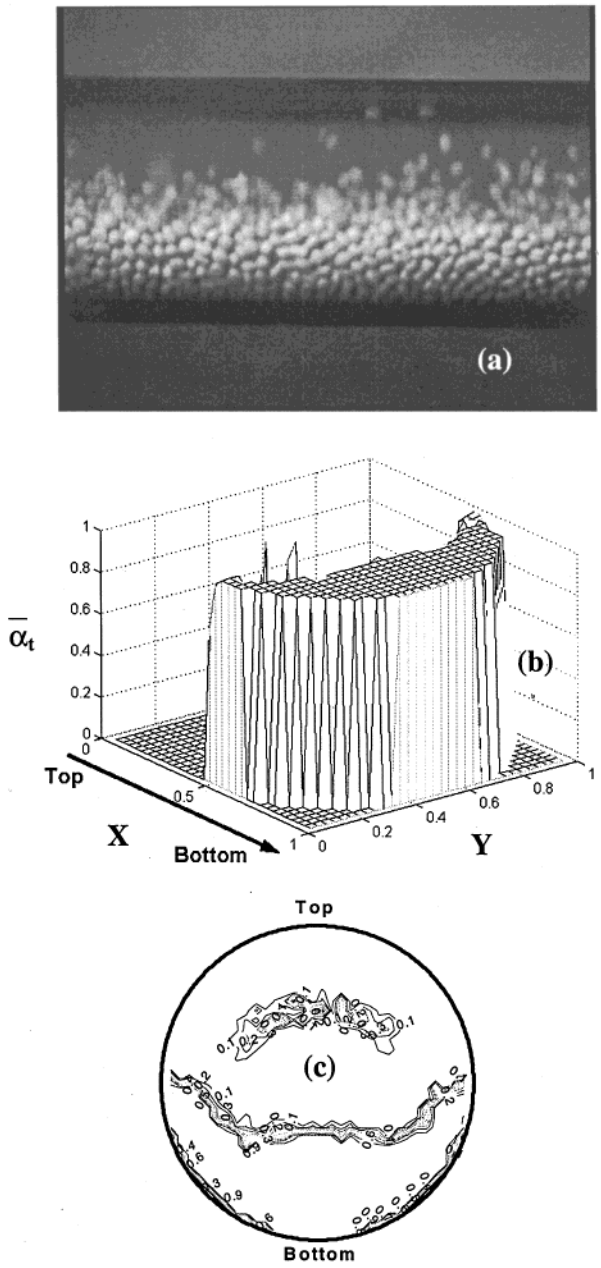

Figure 6. Flow over a settled layer. Air superficial velocity U = 15.6 m/s. Solids feed rate G_s = 17.2 kg/m^2·s (valve opening = 50%, point C in Figure 3b). LLDPE particles: (a) typical flow pattern captured by a video camera; (b) surface plot of time-averaged particle concentration, $\bar{\alpha}_t$; (c) contour plot of $\bar{\alpha}_t$.

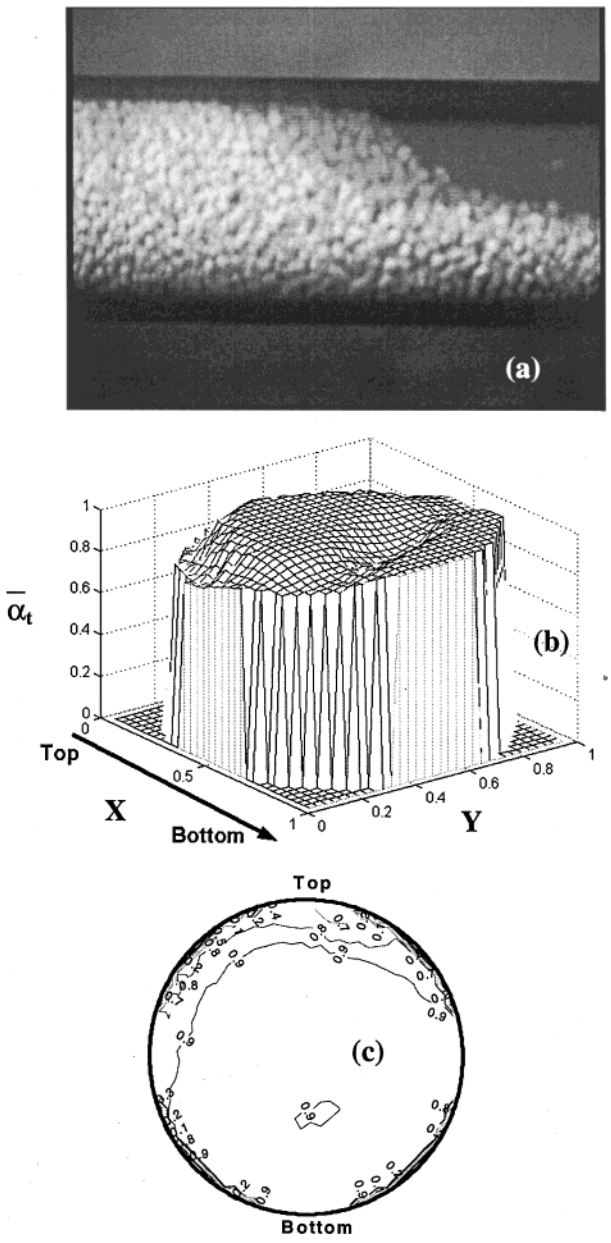

Figure 7. Slug flow regime. Air superficial velocity U = 10.4 m/s. Solids feed rate G_s = 21.1 kg/m^2·s (valve opening = 50%, point D in Figure 3b). LLDPE particles: (a) typical flow pattern captured by a video camera; (b) surface plot of time-averaged particle concentration, $\bar{\alpha}_t$; (c) contour plot of $\bar{\alpha}_t$.

(Brassica Juncea), and polypropylene, whose physical properties are shown in Table 1. Using single-plane ECT data, the time-averaged particle concentration distributions over a cross section of the pipe were determined in various flow regimes, along with temporal variations of the cross-sectional average concentration of particles. The power spectra of these temporal variations were used to fingerprint the flow regimes. With cross correlation of twin-plane ECT data, the propagation velocities of patterns (or simply pattern velocities) were estimated. In general, the pattern velocity is not the same as the average velocity of the particles, and therefore there is no formally correct method to estimate the mass flow rate. A preliminary estimate of the solids mass flow rate may be made by assuming that the average particle velocity is the same as the pattern velocity. We found that mass flow rates estimated in this manner differed systematically from those obtained via load cell measurements and that an ad hoc correction factor that depended on the material being transported through the pipe could be used to obtain the solids flow rate from the ECT data. This is exactly the same idea proposed by Arko et al.[6] for the slug flow regime. Much to our surprise, we found this approach to be accurate within ±20% in other flow regimes as well.

A limited study of flow past a smooth 90° (horizontal-to-vertical) bend was also performed, where we made single-plane ECT measurements to observe the spatial and temporal variation of particle concentrations in the postbend region.

Experimental Section

The schematic layout of the pneumatic conveying facility used in our study is shown in Figure 1**.** The test

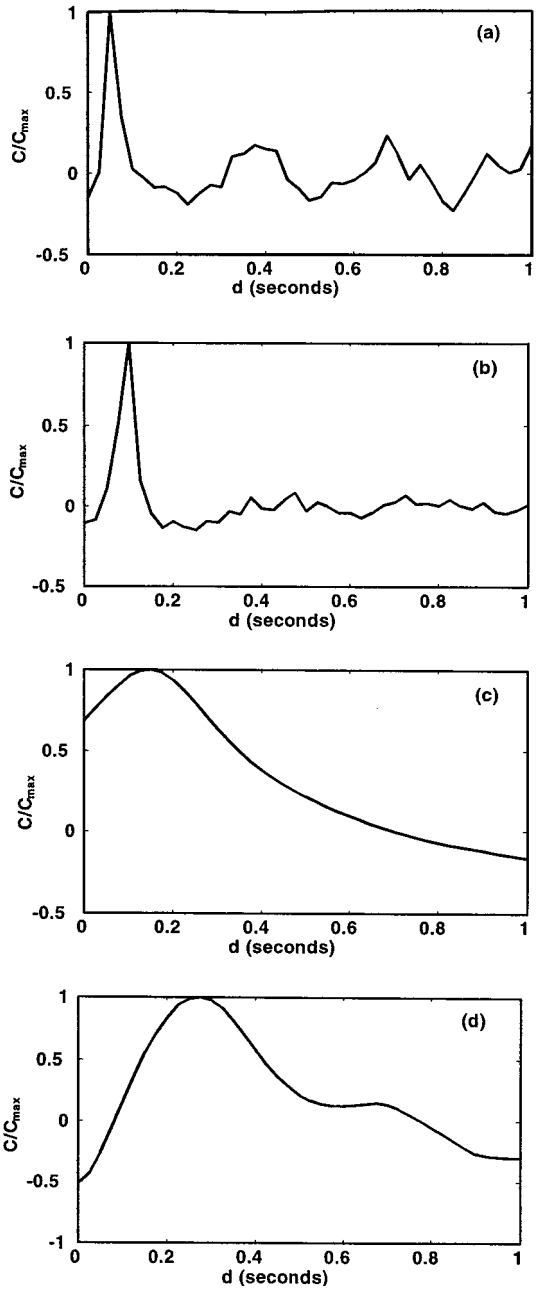

Figure 8. Cross correlation of twin-plane ECT data. The normalized cross-correlation coefficient C/C_{max} is plotted against the delay time d. Here C is given by eq 4 and C_{max} denotes the maximum value of C. (a) Homogeneous flow (Figure 4). (b) Moving dunes (Figure 5). (c) Flow over a settled layer (Figure 6). (d) Slug flow (Figure 7).

rig consisted of a horizontal, 40.4 mm i.d. PVC pipe that is 11.4 m long. One end of this pipe was connected to the outlet of a rotary air-lock feeder (model 152-443 B 12-03 CFR, General Resource Corp., Hopkins, MN) and the other end to a discharge hopper (16 in Figure 1).

The solid particles from the storage hopper (8 in Figure 1) entered the rotary air-lock feeder casing through an intermediate hopper. This hopper arrangement allowed us to maintain a steady supply of solids to the air-lock rotary feeder and also facilitated solids flow rate measurement. A butterfly valve and a diaphragm valve were used to control the solids flux into the air-lock feeder. Compressed air entered the rotary air-lock feeder through a rotameter and entrained the

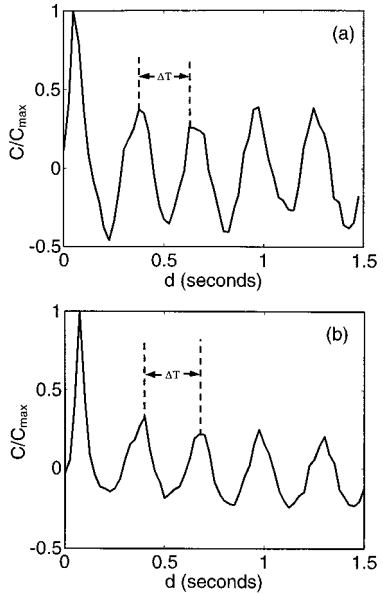

Figure 9. Cross correlation of twin-plane ECT data. The normalized cross-correlation coefficient C/C_{max} is plotted against the delay time d. Homogeneous flow regime. (a) LLDPE particles. Air superficial velocity $U = 28.6$ m/s. Solids feed rate $G_s = 71.4$ kg/m^2·s. (b) Brown mustard. Air superficial velocity $U = 19.5$ m/s. Solids feed rate $G_s = 48.3$ kg/m^2·s. In both figures, $\Delta T \sim 0.3$ s. Frequency $f = 1/\Delta T = 3.3$ Hz.

solid particles along the conveying system. All of the data on horizontal pneumatic conveying reported here were obtained in such a batch mode of operation (because there was no provision for continuously transporting the particles from the discharge hopper to the storage hopper).

Air vents were provided for the two hoppers to avoid pressure buildup in the system. Taps were provided for static pressure transducers (GEMS model K054205 sensors, Basingstone, England) at four locations 0.5, 4.04, 6.84, and 11.04 m away from the feeding end. Pressure data were collected for 30 s, and the mean pressure gradients were determined for different operating conditions. Two 12-electrode (100 mm length) ECT sensors, spaced 0.5 m apart on the horizontal pipe, were mounted for twin-plane measurements. In our experiments on horizontal conveying, the measurements were made under essentially developed flow conditions. ECT sensors were installed at about 4 m away from the feeding point. This corresponds to an L/D ratio of about 100, which is significantly larger than the L/D ratio of 54 used by Arco et al.[6] The pattern propagation velocity was obtained by cross correlation of the twin-plane signals. Figure 2 illustrates the conceptual model of the cross-correlation technique.

The data acquisition module (Process Tomography, Wilmslow, Cheshire, U.K.) together with a computer was connected to the ECT sensors to collect particle concentration data at various air velocities and solids feed rates. A sampling rate of 40 frames/s was employed.

The experiments were conducted in various flow regimes, namely, homogeneous flow, moving dunes, flow over a settled layer, and slug flow. This was achieved by gradually decreasing the air flow rate while keeping the (solids) feed valve opening constant. The measurements were repeated with different valve openings to obtain data at different solid feed rates. The solids flow rate was measured by the conventional

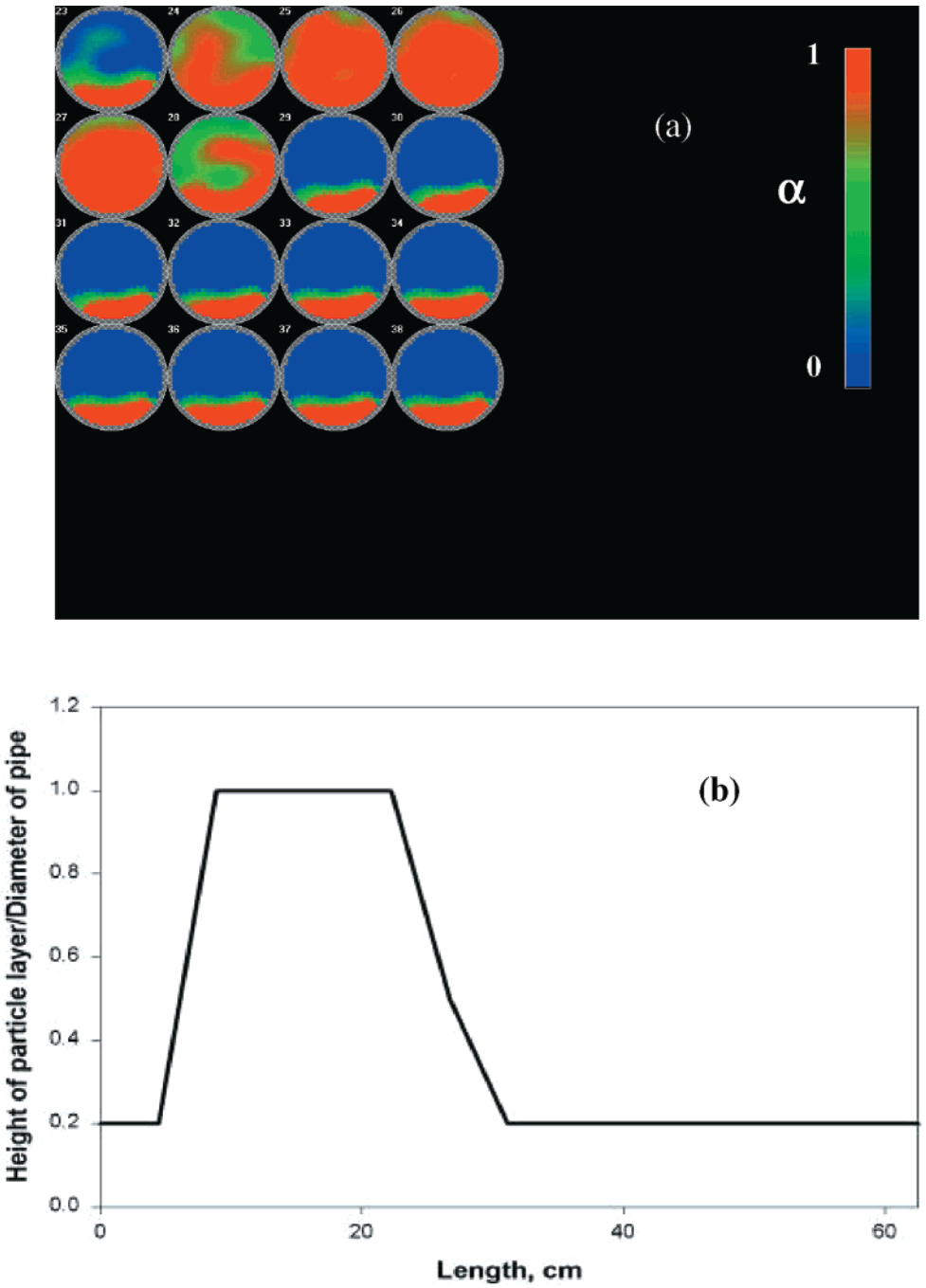

Figure 10. Slug flow of LLDPE particles: (a) sequence of ECT images; (b) reconstructed slug shape. The slug is traveling from right to left.

method of weighing solids at the discharge end for a certain amount of time using an electronic balance (load cell).

At 6.12 m away from the feeding end, the horizontal pipe could be disconnected from the remainder of the horizontal duct and connected via a smooth 90° (r/R = 0.5) bend to a vertical, 40.4 mm i.d. PVC pipe, which, in turn, was connected to the storage hopper through another horizontal PVC pipe. This configuration which represented a continuous mode of operation was used to carry out a limited number of experiments in order to evaluate the ability of ECT to capture temporal and spatial variations in particle concentrations immediately after the bend. In these experiments, one set of ECT sensors was placed before the 90° bend on the horizontal pipe and the other set was located on the vertical riser immediately after the bend.

Results and Discussion

The pneumatic conveying characteristics for the three particles used in our study are shown in Figure 3a−c. In each of these figures, the pressure gradient is plotted against the air superficial velocity (U) for different extents of opening of the solids feed valve. Constant opening of the solids feed valve does not imply constant solids flow rate. Tables 2−4 provide summaries of the air superficial velocity (U), solids mass flux (G_s), and pressure gradient ($\Delta P/L$) corresponding to the data points shown in Figure 3a−c, respectively.

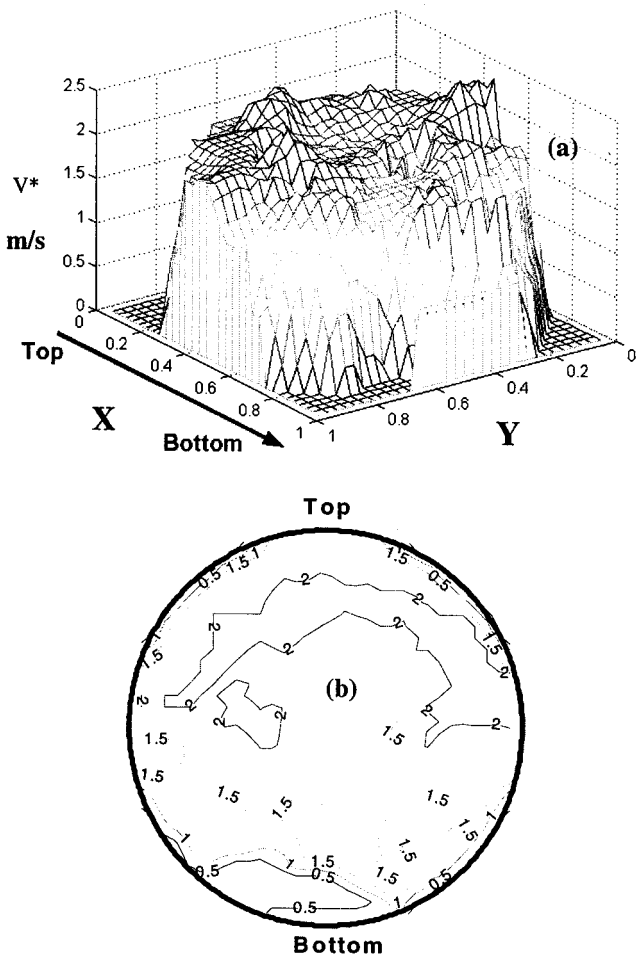

Figure 11. Variation of pattern velocity over the cross section of the pipe. Slug flow regime. LLDPE particles. Air superficial velocity U = 10.4 m/s. Solids mass flux G_s = 21.1 kg/m^2·s. (a) Results presented in the form of a surface plot. (b) Results presented in the form of a contour plot.

Flow Visualization in the Horizontal Pipe. By postprocessing the ECT data at each instant of time (t) using the simultaneous iterative reconstruction technique (SIRT) described by Su et al.,[10] we obtained $\alpha(x,y,z,t)$, which is defined as the local volume fraction of particles divided by the volume fraction of particles at maximum packing (F_p). Here, x and y denote Cartesian coordinates in the cross-sectional plane, made dimensionless using the pipe diameter as the characteristic length, and z is the axial coordinate denoting the location of the ECT electrodes. Henceforth, we will refer to α as the particle concentration. The time-averaged particle concentration ($\bar{\alpha}_t$) was generated by averaging $\alpha(x,y,z,t)$ over a time period T (typically 30 s):

$$\bar{\alpha}_t(x,y,z) = \frac{1}{T}\int_0^T \alpha(x,y,z,t)\, dt \qquad (1)$$

Typical results obtained in various regimes are illustrated in Figures 4−7. Figures 4a−7a show pictures taken using a high-speed video camera, Figures 4b−7b show the corresponding surface plots of $\bar{\alpha}_t$, and Figures 4c−7c represent contour plots of $\bar{\alpha}_t$. At high air superficial velocities (Figure 4), a *homogeneous flow* regime is obtained. Even in this regime, the particle concentration is somewhat higher at the bottom of the pipe as a result of gravitational sedimentation. At somewhat smaller air superficial velocity, the particles are transported in small clusters or dunes along the bottom of the pipe (*moving dunes flow*; Figure 5). The gravitational sedimentation is more pronounced now than in the homogeneous flow regime. At even smaller air superficial velocities, a settled layer of particles (which appears to have a concave shape) forms along the bottom of the pipe (Figure 6), and the particles are mainly transported above the settled layer in the form of particle clouds. If we decrease the air superficial velocity even further, we enter the slug-flow regime (Figure 7), where a number of solid slugs travel intermittently through the pipe with a large fluctuation in pressure and with mechanical vibration. Parts b and c of Figure 7 show the distribution of time-averaged particle concentration over the cross section of the pipe. In this flow pattern, particle concentration distribution is uniformly high with a value close to the maximum possible packing. (Note that the results shown in parts b and c of Figure 7 represent the average over one slug. These results are found to be essentially the same as the average of all four slugs noticed within a sampling period of 30 s.)

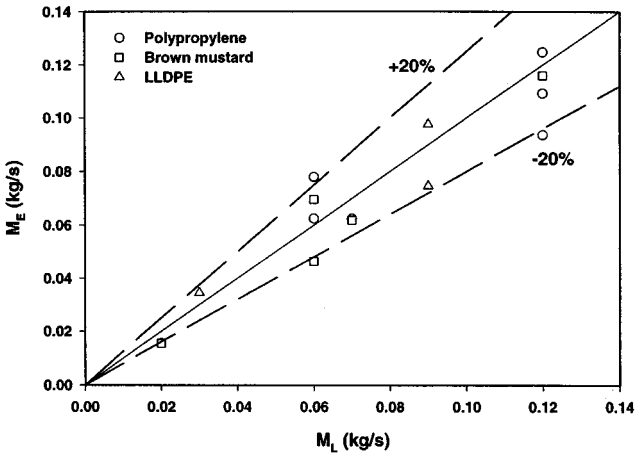

Figure 12. Comparison of mass flow rates estimated from ECT data (M_E, eq 6) with load cell data (M_L).

All of these regimes are well-known, and Figures 4−7 merely reveal that the average particle concentration distributions obtained using ECT are qualitatively correct.

Pattern Velocity Measurements. Twin-plane ECT data were gathered for a variety of operating conditions that covered all of the flow regimes. The cross correlations between signals gathered at the two planes (located at $z = z_1$ and $z = z_2$) were analyzed in two ways. First, we examined how the cross-sectional average particle concentrations at the two planes, $\bar{\alpha}_s(z_1,t)$ and $\bar{\alpha}_s(z_2,t)$, were correlated.

$$\bar{\alpha}_s(z,t) = \frac{1}{A}\int\int \alpha(x,y,z,t)\, dx\, dy \qquad (2)$$

where A is the cross-sectional area of the pipe. The time-averaged value of $\bar{\alpha}_s(z,t)$ is given by

$$\bar{\alpha}(z) = \frac{1}{T}\int_0^T \bar{\alpha}_s(z,t)\, dt \qquad (3)$$

where the averaging was done typically for a period, T, of 30 s. The cross-correlation coefficient, $C(d)$ where d denotes the delay time, was then computed as

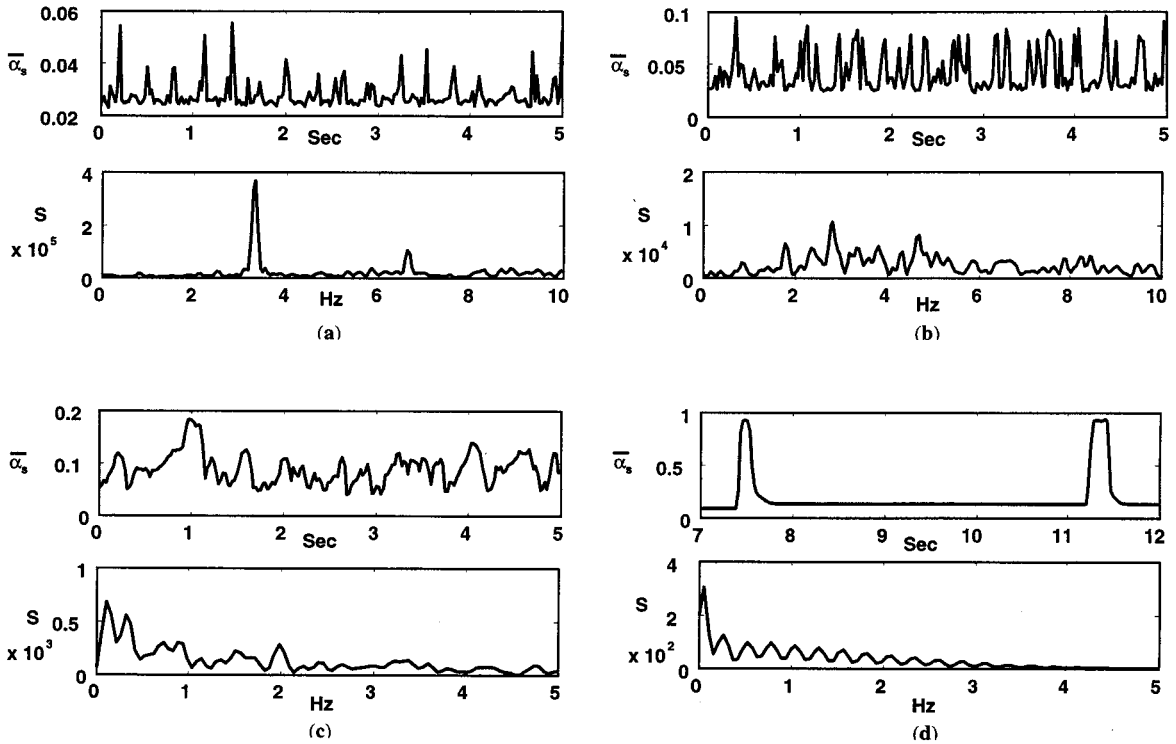

Figure 13. Temporal fluctuations in the concentration of LLDPE particles. $\bar{\alpha}_s$ = cross-sectional average solid concentration. S = power spectrum density. (a) Homogeneous flow (Figure 4). (b) Moving dunes (Figure 5). (c) Flow over a settled layer (Figure 6). (d) Slug flow (Figure 7). Corresponding cross-correlation results are shown in Figure 8.

$$C(d) = \frac{1}{T}\int_0^T [\bar{\alpha}_s(z_1,t) - \bar{\alpha}(z_1)][\bar{\alpha}_s(z_2,t+d) - \bar{\alpha}(z_2)]\,dt \tag{4}$$

Here, z_1 and z_2 refer to upstream and downstream planes, respectively, and d is taken to be positive. The dominant pattern propagation velocity, V^*, was estimated from $V^* = L/D$, where L is the axial distance between the two ECT sensors and D is the value of d at which $C(d)$ is the maximum.

The cross-correlation results for LLDPE particles corresponding to the conditions described earlier in Figures 4−7 are shown in parts a−d of Figure 8, respectively. The estimated pattern velocities for these four cases are 10, 5, 3.33, and 1.78 m/s, respectively. Not surprisingly, the pattern velocity became smaller as the air superficial velocity was decreased.

The cross-correlation coefficient $C(d)$ in the homogeneous flow consistently revealed several smaller peaks (in addition to the dominant one) which were roughly evenly spaced. This is barely visible in Figure 8a but can be seen much more clearly in parts a and b of Figure 9, corresponding to LLDPE and brown mustard particles, respectively. This is indicative of the presence of a periodic wave with a frequency of about 3 Hz. Because a similar frequency signal is observed for both particles, this secondary structure could be due to a disturbance at the inlet of the pipe, i.e., at the junction with the rotary air lock.

Slug Flow. The temporal variation of the particle concentration in the slug flow regime, determined at one of the planes of a twin-plane ECT system, is presented in Figure 10a. The number at the upper left corner indicates the frame count. The red denotes high solids concentration ($\alpha = 1$), whereas the blue corresponds to an empty bed ($\alpha = 0$). Frames 23−29 reveal the passage of a solid slug. From the pattern velocity estimated via cross correlation of the twin-plane ECT data and a frame-by-frame image at one of the planes, one can reconstruct approximately the shape of the slug, and this is illustrated in Figure 10b.

More detailed analysis of the twin-plane ECT data may be performed by computing cross correlation between corresponding pixels in the two planes (i.e., the same x and y). In this manner the dominant pattern velocity can be determined for each pixel. Analyzing in this manner, Arko et al.[6] found the velocity in the slug-flow regime to be quite nonuniform over the cross section of a pipe, with higher (lower) velocity at the upper (lower) portion of the pipe. Our experiments confirm this finding. Figure 11 shows pixel−pixel cross-correlation results for the velocity distribution of particles in the slug across the cross section.

Mass Flow-Rate Estimation. If the particle velocity is assumed to be uniform everywhere and equal to the pattern velocity, the mass flow rates may be estimated readily from the ECT data as (Arko et al.[6])

$$M_E = \rho_s V^* F_p A \bar{\alpha} \tag{5}$$

where ρ_s is the density of particles, A is the cross-sectional area of the conveying pipe, F_p is the packing factor of solids (i.e., particle volume fraction at maximum packing, measured experimentally), and $\bar{\alpha}$ is the average particle concentration.

The actual solids mass flow rates, M_L, were measured independently by weighing solids (load cell measurements) at the discharge end. It was not at all surprising to find that M_E and M_L differed by as much as 50%. However, if eq 5 was modified in an ad hoc manner (Arko et al.[6]) as

$$M_E = f_c \rho_s V^* F_p A \bar{\alpha} \tag{6}$$

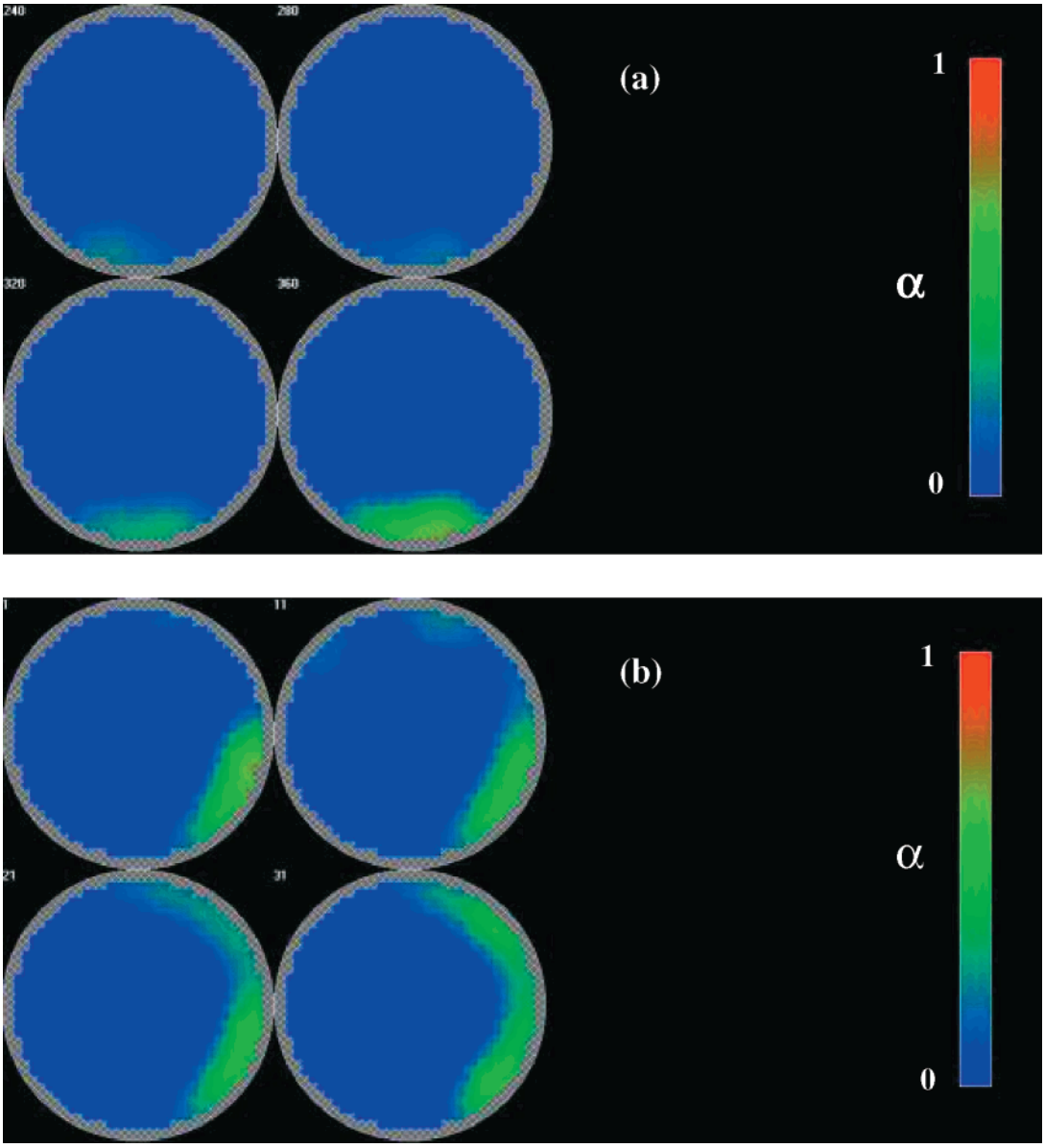

Figure 14. Temporal variation of concentration of LLDPE particles. Flow past a 90° smooth elbow. $U = 15.6$ m/s. $G_s = 20.5$ kg/m^2·s. (a) Four images from ECT data obtained in the horizontal pipe before the bend. This condition lies close to the transition between the regimes of eroding dunes and flow over a settled layer. (b) Four images from ECT data obtained in the vertical pipe shortly after the bend. The presence of a film of particles whose structure is time-dependent is readily seen.

where f_c is an empirical constant to be determined experimentally, M_E and M_L could be brought within ~20% of each other (see Figure 12). We found the correction factor to be different for polypropylene ($f_c = 1.22$; $F_p = 0.77$), LLDPE ($f_c = 0.46$; $F_p = 0.75$), and brown mustard ($f_c = 0.64$; $F_p = 0.72$).

Several factors may contribute to the deviation of ECT mass flow-rate estimates from the classical weighing measurements. These may include errors in concentration measurement, flow pattern characteristics, and errors in particle velocity estimation. Among these, perhaps the most important factor is that the propagation velocity of nonuniformities in the flow is, in general, not equal to average particle velocities. Hence, a material-dependent correction factor f_c is required to estimate the average particle velocity from the measured pattern velocity. The f_c values thus obtained varied from material to material, given by 0.46 for brown mustard, 0.64 for LLDPE, and 1.22 for polypropylene. However, they are all in the same order of 1.

Flow Regime Characterization. The temporal variation of the cross-sectional averaged particle concentration measured by a single-plane ECT system and the corresponding power spectrum are shown in Figure 13a−d for the four different flow regimes. These correspond to Figures 4−7, respectively. Twin-plane ECT results for these operating conditions have been presented earlier in Figure 8.

The presence of fluctuations could be detected even in the homogeneous flow regime (Figure 13a). These fluctuations had a characteristic frequency of ~3 Hz and were already discussed earlier in the context of twin-plane cross-correlation results. This peak could not be seen in the other flow regimes (Figure 13b−d), where it was either absent or too weak to be detected.

Parts b−d of Figure 13 suggest that the regimes of moving dune flow, flow over the settled layer, and slug flow may be identified by the presence of multiple peaks in the 2−5 Hz range, a few dominant peaks in the 0−2 Hz range, and a single dominant low-frequency peak,

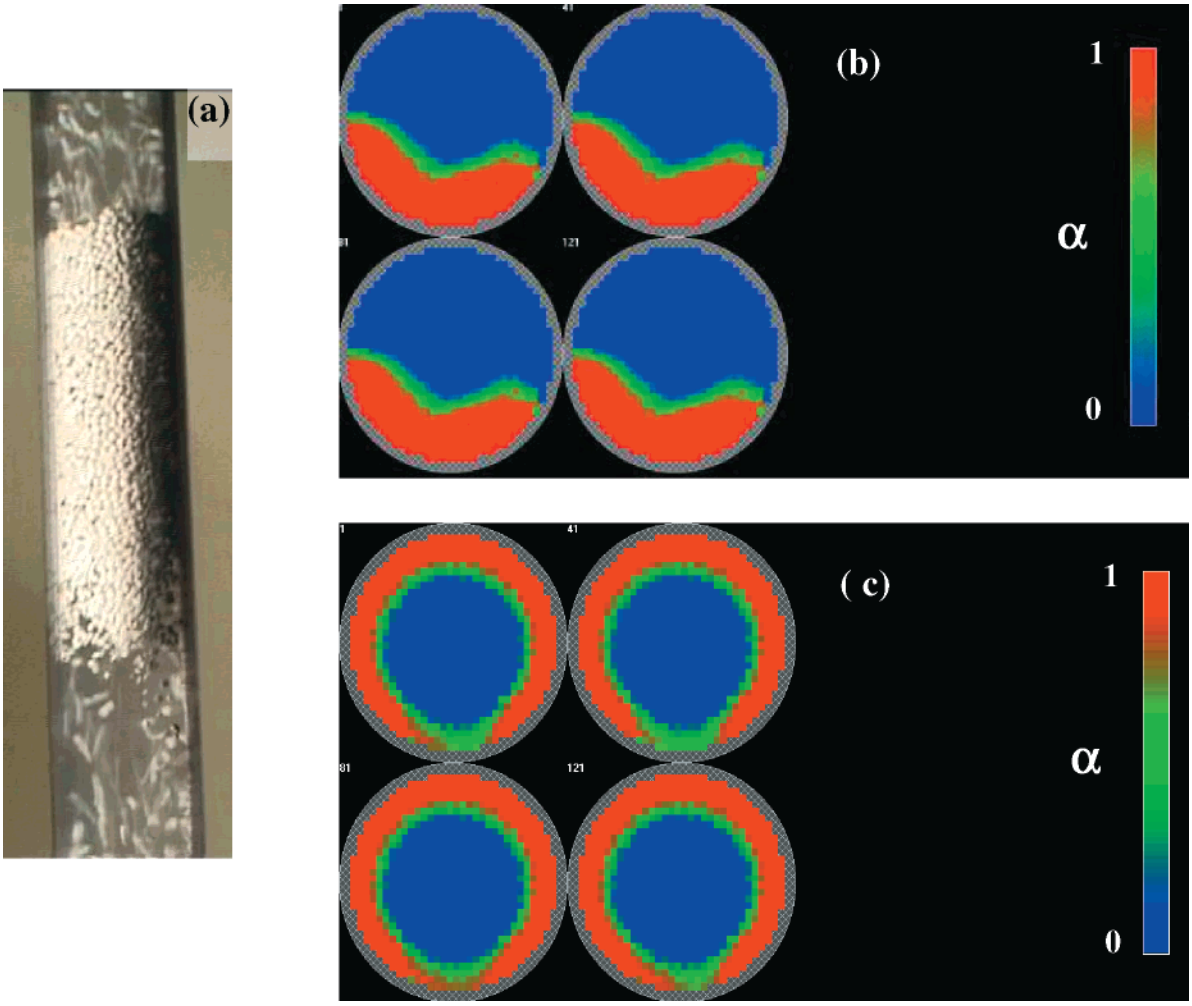

Figure 15. Temporal variation of the concentration of LLDPE particles. Flow past a 90° smooth elbow. $U = 14.3$ m/s. $G_s = 20.5$ kg/m^2·s. (a) Snapshot of a traveling solid layer in the riser pipe. (b) Four images from ECT data obtained in the horizontal pipe before the bend. This condition lies in the regime of flow over a settled layer. (c) Four images from ECT data obtained in the vertical pipe shortly after the bend, showing the ringlike structure.

respectively. The small peaks seen in Figure 13d are simply the higher harmonics of the low-frequency peak.

It is clear from Figure 13a−d that the typical magnitude of the spectral power density, S, increases as the air velocity is decreased. The spectral power density in the regime of moving dunes was typically 1 order of magnitude larger than that in the homogeneous flow regime. Transition to the regime of flow over a settled layer increased it by another order of magnitude, while the next transition to the slug-flow regime resulted in another big increase.

Thus, one may identify the flow regimes either by the fingerprint (as in the frequency range where peaks are found) or the typical magnitude of the spectral power density or both.

Flow through a 90° Bend. We performed a few experiments to test the ability of the ECT system to capture the changes in the distribution of particles over the cross section when particles are conveyed through bends. Two illustrative examples involving conveying of LLDPE particles are presented in Figures 14 and 15 and discussed below.

At high superficial air velocities of about 28.6 m/s (and a solids mass flux of 20.5 kg/m^2·s), the homogeneous flow regime was obtained in the horizontal pipe. We found that flow pattern under these conditions was essentially homogeneous in the vertical riser as well. When the air velocity was brought down to ~15.6 m/s, the flow pattern in the horizontal pipe was close to the transition between the regimes of eroding dunes and flow over a settled layer. Four images from ECT data obtained in the horizontal pipe (with the time elapsed between images being 1 s) before the bend are shown in Figure 14a. This was accompanied by the presence of an unstable film of solids in the vertical riser shortly after the bend. Visual observations revealed that a film of particles formed in the riser leg in a periodic manner and slid down along the wall. As this film approached the bend, it broke up and the particles were transported up through the riser by the air. Four images from ECT data obtained in the vertical pipe shortly after the bend are shown in Figure 14b, and the presence of a time-dependent film of particles is readily seen.

Flow patterns obtained at a somewhat lower air superficial velocity of 14.3 m/s and $G_s = 20.5$ kg/m^2·s are shown in Figure 15. It is clear from the ECT images shown in Figure 15b that the flow pattern in the horizontal pipe was in the regime of flow over a settled layer. Under these conditions, the unstable film of particles which was observed in the riser at the higher air velocity of 15.6 m/s (see Figure 14b) transformed into a ringlike structure (see Figure 15c). A typical photograph of such a ring of particles is shown in the Figure 15a. This ringlike structure extended over a section of

the riser and its location in the riser remained roughly constant, although some local reorganization of individual particles was observed from time to time.

Conclusions

The particle concentration distribution over the cross section of the conveying pipe can be determined from single-plane ECT data in the various flow regimes of pneumatic conveying. Twin-plane ECT data can be used to estimate the corresponding pattern propagation velocities. In the slug-flow regime, the wave shape reconstructed from ECT data was comparable to that obtained using a high-speed video camera.

The dominant pattern velocity obtained from twin-plane ECT data is by no means equal to the average velocity of the solids. Yet, it was found that the solids mass flow rate was roughly proportional to the product of the pattern velocity and the average concentration of particles. However, the proportionality constant had to be found empirically, and it varied appreciably from particle to particle. The present study was restricted to flow in a single horizontal pipe, so it is reasonable to be cautious and expect that the value of the proportionality constant will depend on the pipe diameter and also the pipe orientation. Nevertheless, it seems possible that the solids flow rate could be estimated to within ±20% from ECT data, provided some calibration is done to estimate this constant.

It seems possible to identify the flow regimes on the basis of the temporal variation of the cross-sectional average solids concentration obtained by single-plane ECT measurements, by observing the frequency range where peaks are found and the typical magnitude of the spectral power density.

Acknowledgment

We gratefully acknowledge the financial support for this work from the National University of Singapore (Grant RP960630). We thank Dr. Jinsong Hua and Prof. Reginald B. H. Tan for discussions on the project and Ms. Sofia Lim for technical support.

Nomenclature

A = cross-sectional area of the pipe, m^2
C = cross-correlation coefficient of the particle concentration between planes 1 and 2
C_{max} = maximum correlation coefficient
D = flow transit time (see text after eq 4), s
d = delay time for the cross correlation, s
F_p = volume fraction of particles at maximum packing
f_c = correction factor in eq 6
f = frequency, Hz
G_s = mass flux of solids, $kg/m^2 \cdot s$
L = distance between the two sensing planes; length, m
M_E = mass flow rate estimated by the ECT system, kg/s
M_L = mass flow rate measured by the load cell, kg/s
R = radius of the pipe bend, m
r = inner radius of the pipe, m
S = density of the power spectrum; stratified flow
T = time duration for averaging, s
ΔT = time shift of the periodic wave, s
t = time, s
U = superficial velocity of air, m/s
V^* = pattern velocity, m/s
x, y = dimensionless coordinates in the cross section of a pipe
z = dimensionless coordinate along the axis of the pipe
$\bar{\alpha}_t$ = time-averaged particle concentration
$\bar{\alpha}_s$ = space-averaged particle concentration over a given cross section of the pipe
$\bar{\alpha}$ = space- and time-averaged particle concentration
ρ_s = density of the material, kg/m^3
$\Delta p/L$ = pressure drop per unit length, Pa/m

Literature Cited

(1) Williams, R. A.; Beck, M. S. Introduction to process tomography. *Process Tomography*; Butterworth-Heinemann Ltd.: Boston, 1995.

(2) Hammer, E. A. Three-component flow measurement in oil/gas/water mixtures using capacitance transducers. Ph.D. Thesis, University of Manchester, Manchester, U.K., 1983.

(3) Huang, S. M. Capacitance transducers for component concentration measurement in multicomponent flow process. Ph.D. Thesis, University of Manchester, Manchester, U.K., 1986.

(4) McKee, S. L.; Dyakowski, T.; Williams, R. A.; Bell, T. A.; Allen, T. Solids flow imaging and attrition studies in a pneumatic conveyor. *Powder Technol.* **1995**, *82*, 105−113.

(5) Huang, S. M. Impedance sensors-dielectric systems. In *Process Tomography*; Williams, R. A., Beck M. S., Eds.; Butterworth-Heinemann Ltd.: Boston, 1995.

(6) Arko, A.; Waterfall, R. C.; Beck, M. S.; Dyakowski, T.; Sutcliffe, P.; Byars, M. Development of electrical capacitance tomography for solids mass flow measurements and control of pneumatic conveying systems. *1st World Congress on the Industrial Process tomography*; Buxton: Great Manchester, U.K., April 14−17, 1999; pp 140−146.

(7) Tsuji, Y.; Morikawa, Y. Flow Pattern and Pressure Fluctuation in Air−Solid Two-Phase Flow in a Pipe at Low Air Velocities. *Int. J. Multiphase Flow* **1982**, *8*, 329−341.

(8) Dhodapkar, S. V.; Klinzing, G. E. Pressure Fluctuation in Pneumatic Conveying Systems. *Powder Technol.* **1993**, *74*, 179−195.

(9) Matsumoto, S.; Harakawa, H. Statistical Analysis of the Transition of the Flow Pattern in Vertical Pneumatic Conveying. *Int. J Multiphase Flow* **1987**, *13*, 123−129.

(10) Su, B. L.; Zhang, Y. H.; Peng, L. H.; Yao, D. Y.; Zhang, B. F. The Use of Simultaneous Iterative Reconstruction Technique for Electrical Capacitance Tomography. *Chem. Eng. J.* **2000**, *77*, 37−41.

Received for review January 2, 2001
Revised manuscript received February 26, 2001
Accepted March 7, 2001

IE0100028